Research Article Vol. 32, No. 2 / 15 Jan 2024 / Optics Express 1151
Optics EXPRESS

Propagation effects in polarization-gated attosecond soft-X-ray pulse generation

SAMBIT MITRA,[1,2] JOHANNES SCHÖTZ,[1,2] CHUNMEI ZHANG,[3,4] DONG HYUK KO,[3] ZENGHU CHANG,[5] PAUL B. CORKUM,[3] ANDRÉ STAUDTE,[3] AND MATTHIAS F. KLING[1,2,6,7,*]

[1]*Department of Physics, Ludwig-Maximilians-Universität Munich, Am Coulombwall 1, D-85748 Garching, Germany*
[2]*Max Planck Institute of Quantum Optics, Hans-Kopfermann-Str. 1, D-85748 Garching, Germany*
[3]*Joint Attosecond Science Laboratory, National Research Council of Canada and University of Ottawa, Ottawa, Ontario K1A0R6, Canada*
[4]*Beijing Institute of Technology, No. 5, South Street, Zhongguancun, Haidian District, Beijing, China*
[5]*Institute for the Frontier of Attosecond Science and Technology, The College of Optics and Photonics (CREOL) and Department of Physics, University of Central Florida, Orlando, FL 32816, USA*
[6]*SLAC National Accelerator Laboratory, Menlo Park, CA 94025, USA*
[7]*Applied Physics Department, Stanford University, Stanford, CA 94305, USA*
[*]*kling@stanford.edu*

Abstract: Accurate estimation of the duration of soft-x-ray pulses from high-harmonic generation (HHG) remains challenging given their higher photon energies and broad spectral bandwidth. The carrier-envelope-phase (CEP) dependence of generated soft-x-ray spectra is indicative of attosecond pulse generation, but advanced simulations are needed to infer the pulse duration from such data. Here, we employ macroscopic propagation simulations to reproduce experimental polarization-gated CEP-dependent soft-x-ray spectra. The simulations indicate chirped pulses, which we theoretically find to be compressible in hydrogen plasmas, suggesting this as a viable compression scheme for broadband soft-x-rays from HHG.

© 2024 Optica Publishing Group under the terms of the Optica Open Access Publishing Agreement

1. Introduction

High-harmonic generation (HHG) is a process that inherently converts high-intensity, infrared, or mid-infrared laser pulses into light with higher photon energies [1,2]. The spectral bandwidth of the generated high-harmonic pulses can be large enough to support ultrashort pulses with temporal durations down to even a few attoseconds at their Fourier limit. The shortest pulses currently achieved in the laboratory were measured at 43 attoseconds in the extreme ultraviolet (XUV) spectral region and 53 attoseconds in the soft x-ray spectral region [3,4]. The time-bandwidth product of light generated via HHG indicates, however, a far lower achievable pulse duration, reaching down to ≈ 2.5 as [5] for soft-x-rays. The quest to experimentally obtain even shorter pulses remains an ongoing challenge with an interplay between optimal driving fields, and dispersion compensation of the attosecond pulses, although measuring the spectral phase of the pulse accurately is sufficient for many attosecond measurements [6].

Here, the temporal properties of isolated soft-x-ray attosecond pulses generated by polarization-gated mid-infrared (MIR) laser pulses are numerically explored. These pulses are often used due to their relaxed requirement of the driving pulse duration for the generation of isolated XUV and x-ray pulses [4,7]. The approach used in the simulations has already been successfully employed to model HHG in the XUV to soft-x-ray regime [8–10]. While the exact macroscopic propagation conditions are challenging to reproduce, a qualitative theoretical estimation of the atto-chirp and temporal profile of the soft-x-ray pulses is insightful and hence is included in the simulations. Here, we aim to bridge the gap between previous numerical studies that have

#504636 https://doi.org/10.1364/OE.504636
Journal © 2024 Received 8 Sep 2023; revised 19 Nov 2023; accepted 19 Nov 2023; published 2 Jan 2024

Optics EXPRESS

explored this topic either at the single-atom level [11] or with macroscopic propagation using linearly polarized single-cycle pulses [12]. We focus on simulating HHG by polarization-gated MIR laser fields as they co-propagate in the macroscopic generation medium. Further, the advancement of tabletop long-wavelength laser sources is gradually pushing the spectrum of isolated attosecond pulses toward higher photon energies along with larger bandwidths. As a consequence, traditional pulse retrieval techniques like FROG-CRAB have become error-prone [13] and have led to the development of new pulse retrieval algorithms [14,15]. Simulations based on realistic propagation scenarios provide additional insights into the achievable temporal structure of these isolated attosecond pulses.

To achieve isolated attosecond pulses in time, the laser-field interaction must be modified such that only one laser-field cycle contributes to the emission of the harmonics, unlike multi-cycle emission which leads to a harmonic comb in the spectra and bursts of short pulses in time. Traditionally, such isolation or gating has been achieved by making the driving MIR/IR pulses extremely short in time, such that only one laser cycle is strong enough to produce the highly energetic harmonic emission. Aptly referred to as amplitude gating [16], this approach has been the main route to produce attosecond pulses in the soft x-ray regime [17–20]. A drawback of this method is that it is often challenging to routinely produce ultrashort few-cycle (near single-cycle) MIR/IR laser pulses with high contrast between the central and satellite laser cycles. It leads to isolated attosecond pulses only for the most energetic part of the harmonic spectrum while the lower energy components still exhibit beating in the spectrum due to interference from neighboring attosecond bursts [2]. A carefully chosen metallic filter is necessary in such a scenario to block the lower energy components where multiple bursts are expected, thereby narrowing the total bandwidth of the HHG spectrum.

A less constrained method for the generation of an isolating attosecond pulse is through polarization gating (PG) [21,22]. The harmonic emission is suppressed, as can be understood in the three-step model [23]. After driving the tunneling emission process and accelerating the electron, the electric field rotates suppressing the electron rescattering by making the electron-recollision-trajectory miss the parent ion. Polarization gating is achieved by modifying the polarization of a laser pulse such that the first half of the laser pulse is, e.g., left circularly polarized and the second half is right circularly polarized. This will result in a pulse with a half cycle of linear polarization in the center, as illustrated in Fig. 1.

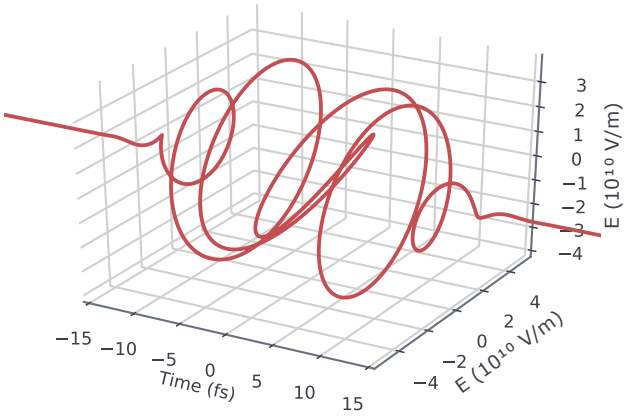

Fig. 1. Time-dependent E-field (along the XY polarization and time axes) of polarization-gated laser pulses used in the numerical simulation.

Optics EXPRESS

2. Numerical modelling

In our model, the field structure of a polarization-gated pulse is realized using the following formalism where the two circularly polarized components are

$$\begin{bmatrix} E_{x1}(t_1) \\ E_{y1}(t_1) \end{bmatrix} = \begin{bmatrix} \sqrt{\frac{2I}{c\epsilon_0}} e^{-2\ln(2)\left(\frac{t_1}{\tau}\right)^2} e^{i2\pi\frac{c}{\lambda}t_1} \\ E_{x1}(t_1)e^{i\frac{\pi}{2}} \end{bmatrix} \tag{1}$$

and

$$\begin{bmatrix} E_{x2}(t_2) \\ E_{y2}(t_2) \end{bmatrix} = \begin{bmatrix} \sqrt{\frac{2I}{c\epsilon_0}} e^{-2\ln(2)\left(\frac{t_2}{\tau}\right)^2} e^{i2\pi\frac{c}{\lambda}t_2} \\ E_{x2}(t_2)e^{-i\frac{\pi}{2}} \end{bmatrix}, \tag{2}$$

where I is the peak intensity, c is the vacuum speed of light, ϵ_0 is the dielectric constant, τ is the pulse duration (FWHM) of the Gaussian envelope, λ is the central wavelength and $t_1 = t - \Delta/2$ ($t_2 = t + \Delta/2$) are the separate time axes where $\Delta = t_2 - t_1$ is the time delay between the two pulses. The combined PG pulse can then be expressed as

$$\begin{bmatrix} E_x(t) \\ E_y(t) \end{bmatrix} = \mathrm{Re}\begin{bmatrix} (E_{x1}(t_1) + E_{x2}(t_2)) \cdot e^{i\Phi_{cep}} \\ (E_{y1}(t_1) + E_{y2}(t_2)) \cdot e^{i\Phi_{cep}} \end{bmatrix} \tag{3}$$

where an additional phase term Φ_{cep} is added to account for the modification of HHG spectra by the CEP. The pulses used here are short enough to see strong CEP-dependence on HHG spectra. The HHG calculation in itself utilizes the strong-field approximation (SFA) [24], and is based on the code developed by Högner and coworkers which includes macroscopic propagation of the computed HHG in the near- and far-field [8,25]. These simulations have proven their versatility by reproducing more recent results on macroscopic effects in HHG driven by MIR laser pulses [9], and CEP dependent or field-tailored two-color driven HHG including propagation effects [10,26].

The pulse used in the simulation is shown in Fig. 1, which is based on realistic parameters that have been experimentally realized. The parameters closely follow experiments reported in [7], where PG MIR pulses were used to produce soft-x-ray harmonics. The carrier wavelength is fixed at 1.7 μm with a pulse duration of 12 fs (Gaussian envelope) and a delay of 11.3 fs between the two circularly polarized pulses is used to produce the desired HHG gate width. The gate width (δ) is expressed as [22]

$$\delta = \frac{\epsilon_t}{\ln(2)} \frac{\tau^2}{\Delta} \tag{4}$$

where $\epsilon_t = 0.1$ is an ellipticity threshold of the laser pulse, where 90% of the harmonic yield drops (in comparison with the linearly polarized case). The value of ϵ_t is taken from [7], where the authors estimate the HHG yield drop using a numerical semi-classical model. The other parameters in Eq. (4) follow the convention as already defined earlier and δ turns out to be 1.8 fs. The value of δ being less than the laser half-cycle (2.8 fs), ensures a single burst of HHG [7,22,27]. In this configuration, the PG pulse (shown in Fig. 1) varies strongly with the CEP, and hence a static CEP of 0.27π is chosen, corresponding to the HHG spectrum with the highest cutoff energies.

In an experiment, the polarization-gated driving laser pulses are focused into a gas medium. This is modeled by first defining a Gaussian focal profile with a beam waist $w_0 = 85$ μm. Further, a neon-gas filled target cell is defined as the generating medium with a thickness of 1.5 mm and a hole size twice that of the Gaussian beam waist. Taking advantage of the cylindrical symmetry of the target, the modeling is done in 2D. A Lorentzian function for the gas density was used to

Optics EXPRESS

account for the gradual decrease in pressure due to gas flowing out of the cell into the vacuum chamber surrounding it, similar to earlier works [9,28]. Figure 2(a) illustrates the phase matching and build-up of the harmonics, integrated over space and frequency as it propagates through the neon target experiencing the pressure gradient of the target. The Gaussian focus of the driving laser is placed 2 mm before the target, motivated by similar experiments where such a position leads to enhanced phase matching of the short trajectories [7]. The observed smooth buildup of harmonics along z justifies the macroscopic parameters chosen in the calculation. Additionally, Fig. 2(b) illustrates the same HHG buildup along z for each photon energy, highlighting a stronger phase-matching in the soft-x-ray region, close to the spectral cutoff ($\approx$ 300 eV). The gas pressure in the simulation was set at 125 mbar, which produced good phase-matching conditions in the target in terms of the HHG yield close to the cutoff energies. Higher pressures resulted in a substantial modification of the MIR driving field and subsequently affected the harmonic buildup over large photon energies in the target. Experimentally, similar configurations have used target gas pressures in the range of 700 mbar – 1 bar [7]. Our previous work showed that phase matching in HHG with MIR drivers sensitively depends on the level of ionization of the target. In modeling the HHG spectra, the ionization level can be controlled by both the ionization rate and the gas pressure. In the simulations, for the ionization rate we used an ADK-based empirical formula for static fields, as proposed by Tong and Lin [29]. It seems that our model provided a slightly too high ionization rate, which we had to compensate for with the lower gas pressure when compared to the experiments.

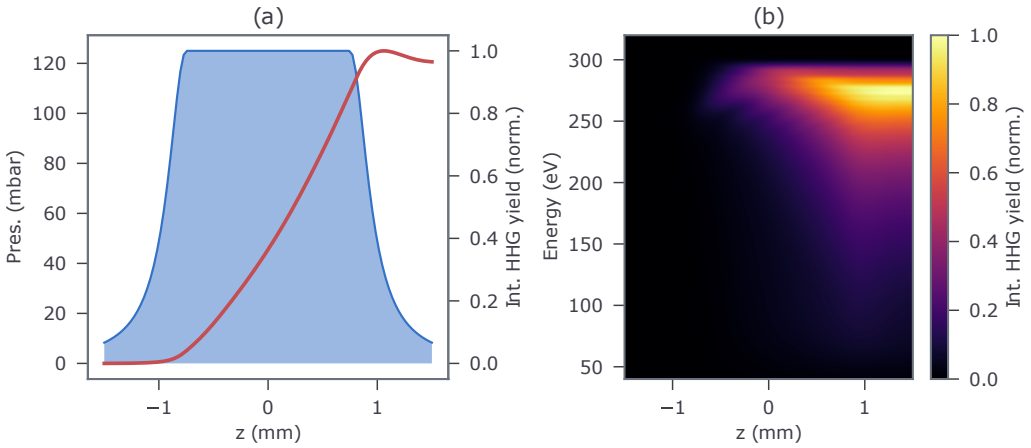

Fig. 2. Phase matching of high harmonics in a neon gas cell with polarization gated MIR driving pulses. a) The Lorentzian gas pressure profile (shaded in blue) used in the simulation along with the HHG yield (red curve) as a function of the propagation distance z, integrated along the frequency and radial axes. b) HHG yield integrated along the radial axis as a function of frequency and propagation length in the gas medium.

Compared to amplitude-gated HHG, an important difference in polarization-gated HHG is the additional ionization, and thereby plasma generation before and after the HHG 'gate'. This occurs as the polarization-gated driving pulses are significantly longer as compared to their amplitude-gated counterpart with the same effective gate width. Looking at the numerical results, this is evident in Fig. 3 where the ionization fraction (red solid line) is observed to significantly increase around the 'gate'. The underlying reason for this is the E-field vector, which, despite being elliptically polarized around the 'gate', does not suppress ionization as highlighted by the dotted red curve in Fig. 3 and has not been accounted for in previous numerical studies in the literature [12].

Optics EXPRESS

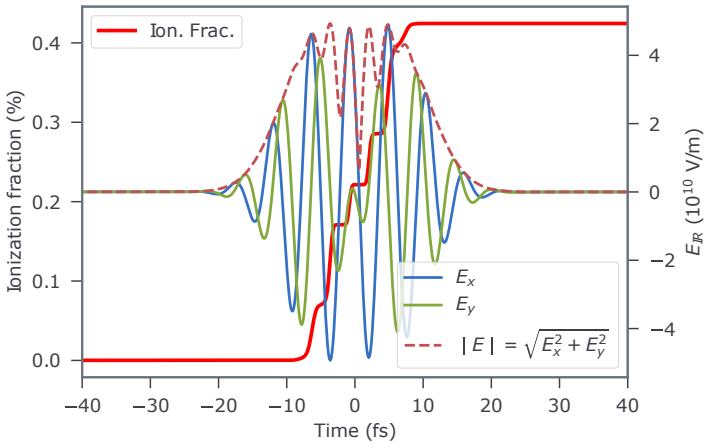

Fig. 3. Ionization fraction at the beginning of the gas target as a function of the time axis of the polarization-gated driving laser field. The E-field in a plane of x-y coordinates exhibits the ellipticity within the pulse which disappears close to the central 'gate' due to a vanishing y component. Additionally, an ellipticity-independent absolute magnitude of the E-field is included to understand the origin of strong ionization around the 'gate'.

3. Results and discussion

With the above-mentioned modification to the driving laser field and generating medium, the effective macroscopic dipole response in the near-field was propagated over 2 m in vacuum. After this propagation step, only the central part of the beam was used to select the low-divergence short trajectory components of HHG [30]. Here, the transmission diameter was 8.4 mm which roughly corresponds to where the signal drops to 40% of the central maxima. HHG experiments routinely used this technique to filter out the short-trajectory harmonics from the negatively chirped, high-divergence longer trajectory harmonics. Additionally, the numerical model used here based on SFA is known to overestimate the contribution of the long-trajectories [31]. As expected, including a larger portion of the spatial profile here led to strong distortion of the temporal profile of the harmonics, and hence was avoided. Finally, the HHG cutoff photon-energy was set at 300 eV to closely match the experimental parameters and the intensity of the driving laser pulse was adjusted accordingly.

The resulting spectrum is shown in Fig. 4(b) along with its spectral phase highlighting a strong second-order positive chirp. As usually observed in HHG experiments [7,32], a thin metallic filter is chosen to block the driving laser field and tailor the HHG spectral phase [33]. A 100-nm thick tin (Sn) filter is therefore included in the numerical modelling for a more accurate estimation of the pulse duration. Hence the spectral distribution below 80 eV is also discarded in the figure as it is fully blocked by the filter [34]. The linearly polarized section (gate) of the polarization-gated laser field (as illustrated in Fig. 1) can rotate in the plane of polarization, leading to the polarization of harmonic emission to experience the same rotation as well, depending on the delay between the two counter-rotating laser pulses. Thus, only the harmonic emission along the polarization axis of the 'gate' of the driving laser pulse is considered for further analysis. Finally, the obtained spectral density is highest around 280 eV while the cutoff energy extends beyond 300 eV, well within the soft-x-ray region.

A Fourier transform of the spectrum including the phase and coupled with a Hilbert transform produces the temporal profile (envelope) of the soft-x-ray pulse as shown by the green curve in Fig. 4(a). For easier representation and comparison, the linear slope of the spectral phase, implying the group delay, has been removed to shift the curve around 0 fs. Here, 0 fs corresponds

Optics EXPRESS

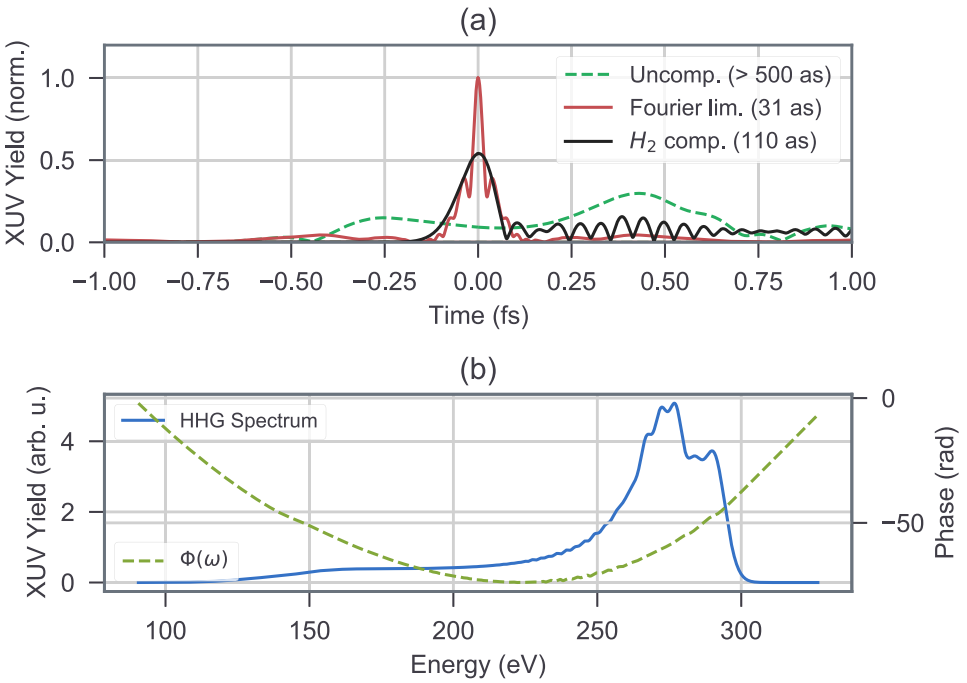

Fig. 4. Simulated temporal and spectral profile of the soft-x-ray attosecond pulses generated by polarization-gated MIR laser pulses in the far-field, after macroscopic propagation through a neon gas cell. (a) A comparison of the temporal structure of the harmonic radiation at its Fourier limit, in its original form and when compressed using H_2-plasma column. (b) The far-field radially integrated numerically obtained dipole spectrum, which is also used to produce the temporal profile of the pulse in (a).

to the center of the driving laser pulse. As expected, the temporal structure appears heavily chirped and extends over 500 as, while its transform limit (with a flat/constant spectral-phase) produces a pulse duration close to an atomic unit of time (24 as) at 31 as (FWHM), and is represented by the red curve in the same figure.

In experiments, the CEP dependence is often considered as an indicator of isolated attosecond pulse generation. In the simulations, the CEP dependence of HHG over large photon energies ranging from 100 eV to the cutoff has been employed as the main parameter to optimize the gas pressure of the generation medium. Higher than optimal gas pressures led to a strong reshaping of the driving laser field and has been discussed in a previous work [12]. In the scenario presented here, high gas pressures lead to laser field reshaping, with its magnitude strongly correlated to the CEP. This results in reduced contrast in the CEP-dependent HHG modulation over the whole spectrum. To prevent field-reshaping, the numerically set gas pressure was gradually reduced until the CEP dependence showed a strong contrast over the whole spectrum (see Fig. 5), and in qualitative agreement with experimental observations [7].

In scenarios where soft-x-ray harmonics are generated, the attosecond bursts are positively chirped due to the mainly surviving short trajectories by their stronger phase-matching and are commonly referred to as atto-chirp [11,35]. The simulations performed here also illustrate this positive chirp and are shown in Fig. 4(b) in terms of the spectral phase along with the spectrum obtained in the far-field after propagation. The origin of chirp in these calculations can be better identified using time-frequency analysis where the different energy components of the harmonic emission can be mapped to when it was emitted on the time axis. The time-frequency map

Optics EXPRESS

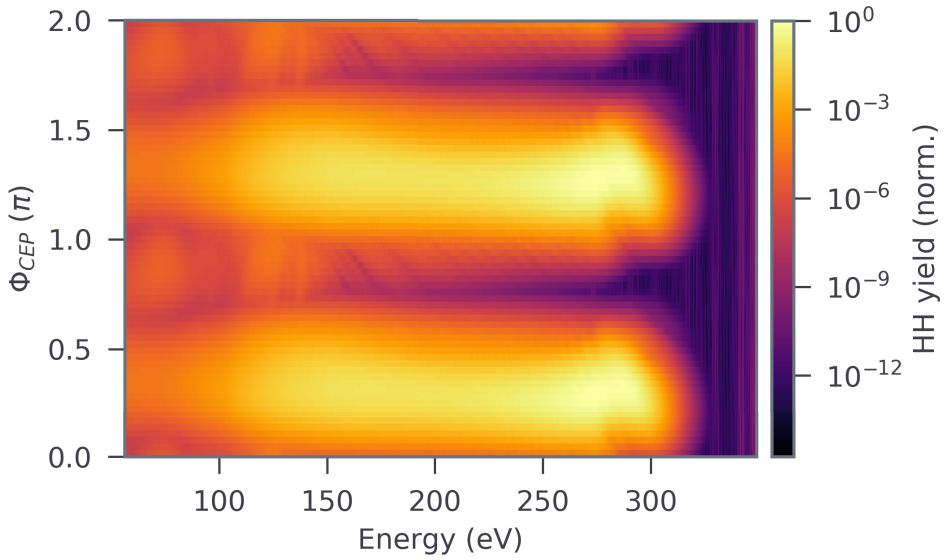

Fig. 5. CEP dependence of polarization-gated HHG in the far-field after macroscopic propagation and radial integration. The spectral distribution also includes the transmission function of a 100-nm thick Sn filter. Unlike other figures, a log scale has been used to represent the HHG yield to highlight the sharp drop for certain CEPs, signifying isolated soft-x-ray pulse generation.

is generated by integrating the harmonic emission over space (radial axis) in the far-field and performing a Short Time Fourier Transform (STFT) with a Hann window (length: 336 as) [36]. The results are shown in Fig. 6 where a characteristic harmonic emission curve is observable within a cycle of the driving laser. The strength of the color map indicates the relative yield in the time-frequency axis and indicates that the short trajectories (indicated by the rising curve and positive chirp) are better phase-matched as compared to the long trajectories (usually present on the falling edge with a negative chirp, after the frequency cutoff). As assumed for the spectrum and temporal profile calculation, the integration over the radial axis here in the far-field also assumes an aperture (see details above), only letting through the central part of the harmonic beam.

The wavelength and intensity dependence of atto-chirp can be derived from a semi-classical three-step model and the approximate estimate near the center of the spectrum is expressed as [11,37]

$$\mathrm{GDD}_{\mathrm{atto}} = 1.63 \times 10^{18} \frac{1}{I_0 \lambda_0} \tag{5}$$

where I_0 and λ_0 are the peak intensity (in $\mathrm{W/cm^2}$) and carrier wavelength (in μm) of the driving pulse, respectively. Although this relationship highlights that the atto-chirp decreases with an increase in wavelength and intensity [38], and hence smaller for MIR wavelengths in comparison to the more commonly available IR ($\approx$ 800 nm) wavelength, the chirp becomes significantly less compressible for photon energies close to 300 eV and above.

Experiments with a spectral density weighted towards lower photon energies (peaking around 150 eV) have been able to use a 400-nm thick tin (Sn) filter to compress the atto-chirp to obtain pulses as short as 53 as [4], characterized using the photo-electron streaking technique [39]. The usability of Sn as a compression material has been found to be limited to below 200 eV [4,33,40], and thus has not been effective in our simulation given the spectral range. The soft-x-ray HHG produced here numerically could not be significantly compressed down in time for thicknesses of

Optics EXPRESS

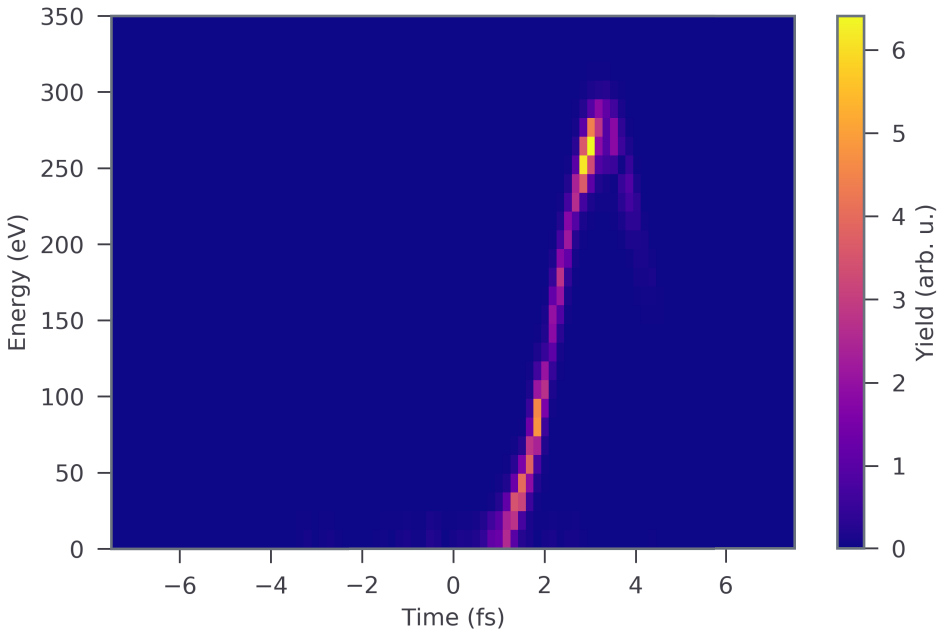

Fig. 6. Time-frequency representation of PG harmonics obtained in the far-field integrated over the radial components. The time axis corresponds to that of the PG MIR laser pulse centered around 0 fs.

the metallic filter (also Sn) up to 1 μm, where the transmission or throughput of HHG is strongly suppressed. The transmission function and the refractive index used to compute the dispersion of x-rays propagating through solids were derived from an atomic scattering factor database [34,41].

Beyond solid-state filters, previous works have experimentally demonstrated the compressibility of HHG in gases either in the generating medium itself, or within a separate gas cell in the XUV spectral region [42,43]. At higher photon energies, there has been a theoretical report where a long column of hydrogen plasma could effectively compress atto-chirp in the range of 300 eV to 1000 eV while still maintaining a relatively high transmission [11]. Following this proposal, the new frequency-dependent refractive index can be expressed as [11]

$$n_{H_2}(\omega) = \sqrt{1 - \frac{\omega_p^2}{\omega^2}} \tag{6}$$

where ω_p is the plasma frequency and is expressed as

$$\omega_p = \sqrt{\frac{e^2 N_e}{\epsilon_0 m_e}} \tag{7}$$

where m_e and e are the mass and charge of an electron, ϵ_0 is the vacuum permittivity, and N_e is the electron density in the plasma, which is approximated to a value of $5{\times}10^{19}\text{cm}^{-3}$ for fully ionized H_2 gas at standard room temperature and pressure [11]. Using the refractive index obtained from Eq. (6), the possibility to compress the spectrum obtained is explored by varying the thickness of the plasma medium d. The shortest temporal profile was obtained with a plasma length of 90 cm, which is close to the value obtained for macroscopic simulations with linearly polarized amplitude gated pulses in the literature [12]. The length can also be shortened if the gas pressure inside is increased as the product of the pressure and length determines the dispersion compensation in

Optics EXPRESS

the medium [11]. Finally, a compressed pulse duration of 110 as (FWHM) is obtained and is represented by the black curve in Fig. 4 (a). As evident, this is still significantly larger than the Fourier limit. The dispersion parameters of the simulated pulses were extracted by fitting a Taylor series to the spectral phase of the pulse before and after compression. We obtained GDD=6705 as^2, TOD=9115 as^3, FOD=-1092056 as^4 before compression and GDD=832 as^2, TOD=67593 as^3, and FOD=-2682691 as^4 after compression. The analysis shows that the increase in TOD and FOD limited further shortening of the pulses. A similar distortion was also observed in the experimentally demonstrated compression using a Sn filter [4].

4. Conclusions

In conclusion, full 3D numerical simulations based on the SFA including macroscopic propagation were performed in both orthogonal polarization axes enabling realistic modeling of soft-x-ray HHG driven by a polarization-gated pulse. The laser and HHG medium parameters were closely based on previous experimental work [7]. The simulations could reproduce the experimental results, including the CEP dependence of the HHG spectra. The attosecond pulses could be compressed by a 90 cm long channel of H_2 plasma, as proposed earlier in the literature [11]. Although this may look challenging experimentally at a first glance, H_2-plasma capillaries have been demonstrated in the past [44,45]. Despite this, as also observed in the single atom calculations [11], the pulse obtained is not fully compressible close to its Fourier limit due to the residual higher-order dispersion of the attosecond pulse. Compensation of higher order dispersion in the soft x-ray region remains an open problem for further investigations with alternate compression schemes.

Funding. Max-Planck-Gesellschaft (Max Planck Fellow program, IMPRS-APS); Office of Science (DE-AC02-338 76SF00515, DE-SC0063).

Acknowledgments. We acknowledge fruitful discussions about the simulation code with Maximilian Högner. S.M. and J.S. acknowledge support from the Max Planck Society via the IMPRS for Advanced Photon Science. M.F.K.'s work at SLAC is supported by the U.S. Department of Energy, Office of Science, Basic Energy Sciences, under DE-AC02-76SF00515 and DE-SC0063.

Disclosures. The authors declare no conflicts of interest.

Data availability. Data underlying the results presented in this paper are not publicly available at this time but may be obtained from the authors upon reasonable request.

References

1. P. B. Corkum and F. Krausz, "Attosecond science," Nat. Phys. **3**(6), 381–387 (2007).
2. F. Krausz and M. Ivanov, "Attosecond physics," Rev. Mod. Phys. **81**(1), 163–234 (2009).
3. T. Gaumnitz, A. Jain, Y. Pertot, *et al.*, "Streaking of 43-attosecond soft-x-ray pulses generated by a passively CEP-stable mid-infrared driver," Opt. Express **25**(22), 27506 (2017).
4. J. Li, X. Ren, Y. Yin, *et al.*, "53-attosecond x-ray pulses reach the carbon k-edge," Nat. Commun. **8**(1), 186 (2017).
5. D. Popmintchev, B. R. Galloway, M.-C. Chen, *et al.*, "Near- and extended-edge x-ray-absorption fine-structure spectroscopy using ultrafast coherent high-order harmonic supercontinua," Phys. Rev. Lett. **120**(9), 093002 (2018).
6. K. Ohmori, H. Katsuki, H. Chiba, *et al.*, "Real-time observation of phase-controlled molecular wave-packet interference," Phys. Rev. Lett. **96**(9), 093002 (2006).
7. J. Li, X. Ren, Y. Yin, *et al.*, "Polarization gating of high harmonic generation in the water window," Appl. Phys. Lett. **108**(23), 231102 (2016).
8. M. Högner, V. Tosa, and I. Pupeza, "Generation of isolated attosecond pulses with enhancement cavities–a theoretical study," New J. Phys. **19**(3), 033040 (2017).
9. J. Schötz, B. Förg, W. Schweinberger, *et al.*, "Phase-matching for generation of isolated attosecond xuv and soft-x-ray pulses with few-cycle drivers," Phys. Rev. X **10**(4), 041011 (2020).
10. S. Mitra, S. Biswas, J. Schötz, *et al.*, "Suppression of individual peaks in two-colour high harmonic generation," J. Phys. B: At., Mol. Opt. Phys. **53**(13), 134004 (2020).
11. Z. Chang, "Attosecond chirp compensation in water window by plasma dispersion," Opt. Express **26**(25), 33238–33244 (2018).
12. K. Kovács and V. Tosa, "Macroscopic attosecond chirp compensation," Opt. Express **27**(15), 21872 (2019).
13. Y. Mairesse and F. Quéré, "Frequency-resolved optical gating for complete reconstruction of attosecond bursts," Phys. Rev. A **71**(1), 011401 (2005).

Optics EXPRESS

14. M. Chini, S. Gilbertson, S. D. Khan, *et al.*, "Characterizing ultrabroadband attosecond lasers," Opt. Express **18**(12), 13006 (2010).
15. S. Pabst and J. M. Dahlström, "Characterizing attosecond pulses in the soft x-ray regime," J. Phys. B: At., Mol. Opt. Phys. **50**(10), 104002 (2017).
16. M. Hentschel, R. Kienberger, C. Spielmann, *et al.*, "Attosecond metrology," Nature **414**(6863), 509–513 (2001).
17. N. Ishii, K. Kaneshima, K. Kitano, *et al.*, "Sub-two-cycle, carrier-envelope phase-stable, intense optical pulses at 16 μm from a BiB_3o_6optical parametric chirped-pulse amplifier," Opt. Lett. **37**(20), 4182 (2012).
18. S. L. Cousin, N. Di Palo, B. Buades, *et al.*, "Attosecond streaking in the water window: A new regime of attosecond pulse characterization," Phys. Rev. X **7**(4), 041030 (2017).
19. S. M. Teichmann, F. Silva, S. L. Cousin, *et al.*, "0.5-keV soft x-ray attosecond continua," Nat. Commun. **7**(1), 11493 (2016).
20. N. Ishii, K. Kaneshima, K. Kitano, *et al.*, "Carrier-envelope phase-dependent high harmonic generation in the water window using few-cycle infrared pulses," Nat. Commun. **5**(1), 3331 (2014).
21. P. B. Corkum, N. H. Burnett, and M. Y. Ivanov, "Subfemtosecond pulses," Opt. Lett. **19**(22), 1870 (1994).
22. Z. Chang, "Single attosecond pulse and xuv supercontinuum in the high-order harmonic plateau," Phys. Rev. A **70**(4), 043802 (2004).
23. P. B. Corkum, "Plasma perspective on strong field multiphoton ionization," Phys. Rev. Lett. **71**(13), 1994–1997 (1993).
24. M. Lewenstein, P. Balcou, M. Y. Ivanov, *et al.*, "Theory of high-harmonic generation by low-frequency laser fields," Phys. Rev. A **49**(3), 2117–2132 (1994).
25. M. Högner, "Spatio-spectrally tailored nonlinear enhancement cavities," Ph.D. thesis, Ludwig-Maximilians-Universität München (2019).
26. S. Mitra, "Strong-field physics in tailored light," Ph.D. thesis, Ludwig-Maximilians-Universität München (2023).
27. Z. Chang, "Chirp of the single attosecond pulse generated by a polarization gating," Phys. Rev. A **71**(2), 023813 (2005).
28. A. Ansari, M. Kumar, H. Singhal, *et al.*, "The effect of gas-density gradient on high-harmonic generation from neon-filled cells using annular and gaussian laser beams," J. Phys. B: At., Mol. Opt. Phys. **55**(16), 165602 (2022).
29. X. M. Tong and C. D. Lin, "Empirical formula for static field ionization rates of atoms and molecules by lasers in the barrier-suppression regime," J. Phys. B: At., Mol. Opt. Phys. **38**(15), 2593–2600 (2005).
30. S. Roscam Abbing, F. Campi, F. S. Sajjadian, *et al.*, "Divergence control of high-harmonic generation," Phys. Rev. Appl. **13**(5), 054029 (2020).
31. M. B. Gaarde and K. J. Schafer, "Quantum path distributions for high-order harmonics in rare gas atoms," Phys. Rev. A **65**(3), 031406 (2002).
32. R. López-Martens, K. Varjú, P. Johnsson, *et al.*, "Amplitude and phase control of attosecond light pulses," Phys. Rev. Lett. **94**(3), 033001 (2005).
33. D. H. Ko, K. T. Kim, and C. H. Nam, "Attosecond-chirp compensation with material dispersion to produce near transform-limited attosecond pulses," J. Phys. B: At., Mol. Opt. Phys. **45**(7), 074015 (2012).
34. B. Henke, E. Gullikson, and J. Davis, "X-ray interactions: Photoabsorption, scattering, transmission, and reflection at e = 50-30,000 ev, z = 1-92," At. Data Nucl. Data Tables **54**(2), 181–342 (1993).
35. S. Kazamias and P. Balcou, "Intrinsic chirp of attosecond pulses: Single-atom model versus experiment," Phys. Rev. A **69**(6), 063416 (2004).
36. D. Griffin and J. Lim, "Signal estimation from modified short-time fourier transform," IEEE Trans. Acoust., Speech, Signal Process. **32**(2), 236–243 (1984).
37. Z. Chang, *Fundamentals of Attosecond Optics* (CRC Press, 2016).
38. G. Doumy, J. Wheeler, C. Roedig, *et al.*, "Attosecond synchronization of high-order harmonics from midinfrared drivers," Phys. Rev. Lett. **102**(9), 093002 (2009).
39. J. Itatani, F. Quéré, G. L. Yudin, *et al.*, "Attosecond streak camera," Phys. Rev. Lett. **88**(17), 173903 (2002).
40. K. T. Kim, C. M. Kim, M.-G. Baik, *et al.*, "Single sub–50–attosecond pulse generation from chirp-compensated harmonic radiation using material dispersion," Phys. Rev. A **69**(5), 051805 (2004).
41. B. L. Henke, J. A. Smith, and D. T. Attwood, "0.1–10-keV x-ray-induced electron emissions from solids—models and secondary electron measurements," J. Appl. Phys. **48**(5), 1852–1866 (1977).
42. K. T. Kim, K. S. Kang, M. N. Park, *et al.*, "Self-compression of attosecond high-order harmonic pulses," Phys. Rev. Lett. **99**(22), 223904 (2007).
43. D. H. Ko, K. T. Kim, J. Park, *et al.*, "Attosecond chirp compensation over broadband high-order harmonics to generate near transform-limited 63 as pulses," New J. Phys. **12**(6), 063008 (2010).
44. A. Butler, D. J. Spence, and S. M. Hooker, "Guiding of high-intensity laser pulses with a hydrogen-filled capillary discharge waveguide," Phys. Rev. Lett. **89**(18), 185003 (2002).
45. A. J. Gonsalves, F. Liu, N. A. Bobrova, *et al.*, "Demonstration of a high repetition rate capillary discharge waveguide," J. Appl. Phys. **119**(3), 033302 (2016).